

# Superconductivity on a quasiperiodic lattice: Extended-to-localized crossover of Cooper pairs

Shiro Sakai,<sup>1</sup> Nayuta Takemori,<sup>1</sup> Akihisa Koga,<sup>2</sup> and Ryotaro Arita<sup>1</sup>

<sup>1</sup>Center For Emergent Matter Science, RIKEN, Wako, Saitama 351-0198, Japan

<sup>2</sup>Department of Physics, Tokyo Institute of Technology, Meguro, Tokyo 152-8551, Japan

(Received 12 August 2016; revised manuscript received 20 November 2016; published 18 January 2017)

We study a possible superconductivity in quasiperiodic systems by portraying the issue within the attractive Hubbard model on a Penrose lattice. Applying a real-space dynamical mean-field theory to the model consisting of 4181 sites, we find a superconducting phase at low temperatures. Reflecting the nonperiodicity of the Penrose lattice, the superconducting state exhibits an inhomogeneity. According to the type of the inhomogeneity, the superconducting phase is categorized into three different regions which cross over each other. Among them, the weak-coupling region exhibits spatially extended Cooper pairs, which are nevertheless distinct from the conventional pairing of two electrons with opposite momenta.

DOI: 10.1103/PhysRevB.95.024509

Quasicrystal is a crystal without translational symmetry. Prominent spots observed in its diffraction pattern manifest an orderly structure while they do not conform to any periodicity. An example of such structures holds the icosahedral point-group symmetry, as first discovered by Shechtman *et al.* [1], and various other structures have hitherto been reported [2–4]. These structures may originate novel electronic properties distinct from those of conventional periodic crystals. In fact, previous theoretical works revealed various nontrivial properties, such as the presence of a confined state [5,6], fractal dimensions [7–9], singular continuous spectral measure [8,10,11], pseudogap in the density of states [12], and a conductance decaying in power of system size [13,14], for free electrons on the quasiperiodic lattices. Moreover, recent observation of quantum critical behavior in Au<sub>51</sub>Al<sub>34</sub>Yb<sub>15</sub> [15] has stimulated theoretical studies [16–25] on the role of electron correlations in these systems.

Another interesting recent observation is a superconductivity in approximant crystals (i.e., periodic crystals with the same local structure as the quasicrystals), Au<sub>64</sub>Ge<sub>22</sub>Yb<sub>14</sub> and Au<sub>63.5</sub>Ge<sub>20.5</sub>Yb<sub>16</sub> [26]. A superconductivity has also been reported in Al-Cu-(Mg, Li) quasicrystalline alloys [27,28]. These observations raise fundamental questions about a possible superconductivity in quasicrystals: How can a superconductivity emerge in a system without translational symmetry? If it exists, what differs from the superconductivity in periodic systems? These questions also have a relevance to experiment of ultracold atomic gases, for which optical quasiperiodic lattices have been available [29–32].

According to an early consideration by Anderson [33] about the impurity effect on superconductivity, Cooper pairs can exist in principle even in the absence of the translational symmetry. In this case, an electron finds its partner in the time-reversed state, which is a generalization of the standard pairing of  $\mathbf{k} \uparrow$  and  $-\mathbf{k} \downarrow$ . However, as a matter of course, this does not guarantee the presence of superconductivity in quasiperiodic systems. This many-body problem requires an explicit calculation taking into account both the pairing interaction and the lattice geometry.

In this paper we address the above issues in a simple setting, i.e., the attractive Hubbard model on a Penrose lattice [34]. On periodic lattices, the attractive Hubbard model is known

to show the superconductivity at any finite value of the attraction  $U < 0$  in the ground state while the character of the superconducting transition changes with  $U$  [35]: For small  $|U|$  (typically smaller than the bandwidth), it follows well the Bardeen-Cooper-Schrieffer (BCS) theory [36] while for large  $|U|$  it behaves like a Bose-Einstein condensation (BEC) of incoherent pairs performed above the transition temperature.

We study the attractive Hubbard model on the Penrose lattice within the real-space dynamical mean-field theory (RDMFT) [20,37–39] explained below. At low temperatures, we find a superconducting phase in a wide range of  $U$  and electron density. The on-site pair amplitude shows a site dependence, yielding various spatial patterns depending on the electron density and  $U$ . Analyzing them, we find three distinct regions, which cross over each other, within the superconducting phase; (i) weak-coupling region, where the Cooper pairs are spatially extended, (ii) low-density and strong-coupling region, where the BEC picture holds aside from the electron-density modulation, and (iii) high-density and strong-coupling region, where the density modulation is relatively weak and the Cooper pairs are short ranged. We show that the superconducting state (i) reflects the geometry of the Penrose lattice most strongly and constitutes a new pairing state which departs from both the BCS and BEC pictures.

The Hubbard Hamiltonian reads

$$H = -t \sum_{(ij)\sigma} c_{i\sigma}^\dagger c_{j\sigma} - \mu \sum_{i\sigma} n_{i\sigma} + U \sum_i n_{i\uparrow} n_{i\downarrow}, \quad (1)$$

where  $c_{i\sigma}$  ( $c_{i\sigma}^\dagger$ ) annihilates (creates) an electron of spin  $\sigma$  at site  $i$  on the two-dimensional Penrose lattice and  $n_{i\sigma} \equiv c_{i\sigma}^\dagger c_{i\sigma}$ .  $t$  is the transfer integral between the nearest-neighbor sites  $\langle ij \rangle$  and  $\mu$  is the chemical potential. We consider an open-boundary cluster of  $N = 4181$  sites, generated by iteratively applying the inflation-deflation rule [40]. The cluster holds a fivefold rotational symmetry as illustrated in Fig. 1. We take  $t = 1$  as the unit of energy. At  $U = 0$ , the difference between the highest and lowest eigenenergies (i.e., the “bandwidth”) is about 8.46, which is close to the value (8.47) estimated for the infinite lattice [5]. We have chosen the two-dimensional lattice, rather than three-dimensional one, in order to study a long-range behavior reflecting the quasiperiodicity.

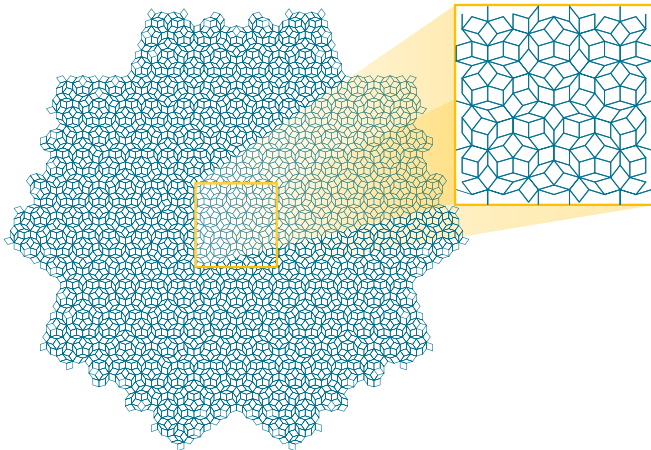


FIG. 1. Two-dimensional Penrose lattice of 4181 sites. The sites are located at vertices of rhombuses. Top-right panel is an enlarged view of a part of the lattice.

In the RDMFT, the effective impurity model is defined and solved at each symmetrically independent site (which amounts to 444 sites for  $N = 4181$ ). As the impurity solver, we use a finite-temperature exact-diagonalization (ED) method [41,42] extended to the superconducting state [43,44]. The calculated local self-energy  $\Sigma_i$  has a dependence on the site index  $i$  while the nonlocal self-energies are neglected.

In the superconducting state,  $\Sigma_i$  is a  $2 \times 2$  Nambu matrix while here we use a plain notation just for the sake of brevity. We define the lattice Green's function  $\hat{G}_{\text{lat}}$  as a real-space matrix:

$$[\hat{G}_{\text{lat}}(i\omega_n)^{-1}]_{ij} = [i\omega_n\sigma_0 + \mu\sigma_3 - \Sigma_i(i\omega_n)]\delta_{ij} - t\sigma_3\delta_{(ij)}, \quad (2)$$

where  $\omega_n = (2n + 1)\pi T$  is the Matsubara frequency at a temperature  $T$ , and  $\sigma_{0,3}$  is the Pauli matrix.  $\delta_{(ij)} = 1$  for nearest-neighbor sites  $\langle ij \rangle$  and 0 otherwise. Taking the matrix inverse of the right-hand side of Eq. (2), we obtain Green's function reflecting the hopping structure of the Penrose lattice. The dynamical mean field  $g_i^0(i\omega_n)$  at each site  $i$  is determined self-consistently by

$$g_i^0(i\omega_n) = \{[\hat{G}_{\text{lat}}(i\omega_n)^{-1}]_{ii} + \Sigma_i(i\omega_n)\}^{-1}. \quad (3)$$

In order to apply ED, we fit  $g_i^0(i\omega_n)$  with a function involving six bath sites, which indeed give a sufficiently accurate fitting for the parameters studied in this paper.

The RDMFT can describe both the BCS and BEC regimes on equal footing [43,45–49]. Although the RDMFT neglects the spatial fluctuations, we take this approach to study the sufficiently large cluster reflecting the quasiperiodicity of our primary interest, at sacrifice of two dimensionality.

Figure 2 shows that the on-site superconducting order parameter  $\text{OP}_i \equiv \langle c_{i\uparrow}c_{i\downarrow} \rangle$  indeed becomes finite at low  $T$  [50]. The phase of  $\text{OP}_i$  is always found to be uniform in space (so that we take all  $\text{OP}_i$ 's to be positive hereafter) while its amplitude depends on sites as represented by the scattering red crosses. Despite the inhomogeneity in  $\text{OP}_i$ , the normal-to-superconducting transition occurs simultaneously at every site within the precision of the present calculation [Fig. 2(a)]. The

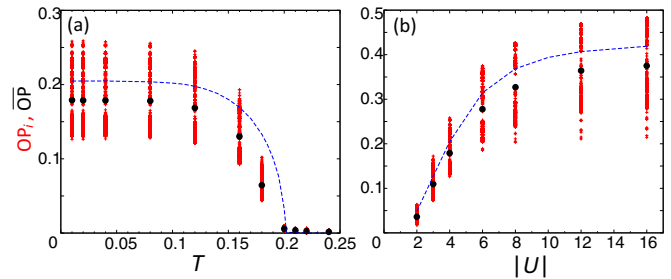


FIG. 2. (a)  $T$  dependence of  $\text{OP}_i$  (red crosses) and  $\overline{\text{OP}}$  (black dots) for  $\bar{n} = 0.5$  and  $U = -4$ . Blue curve plots the DMFT results for the Bethe lattice with the bandwidth  $8t$  at quarter filling. (b) The same for  $U$  dependence for  $\bar{n} = 0.5$  and  $T = 0.01$ .

mean value  $\overline{\text{OP}} \equiv \frac{1}{N} \sum_{i=1, \dots, N} \text{OP}_i$  (denoted by black dots) increases monotonically with  $|U|$ , similarly to the case of the Bethe lattice in infinite dimensions (blue dashed curve) [Fig. 2(b)]. Note that the transition temperature and  $\overline{\text{OP}}$  show scales similar to those of the Bethe lattice with a similar bandwidth.

Figure 3 depicts the spatial patterns of  $\text{OP}_i$ , as well as of  $n_i \equiv \sum_{\sigma} \langle n_{i\sigma} \rangle$ , at  $T = 0.01$ . The patterns change with  $U$  and the average density  $\bar{n} \equiv \frac{1}{N} \sum_{i=1, \dots, N} n_i$ , holding a fivefold rotational symmetry. Here we show three distinct examples. Figure 3(a) shows a representative result for a weak coupling, where  $\overline{\text{OP}}$  is not large [see Fig. 2(b)]. While  $n_i$  clearly shows an orderly structure,  $\text{OP}_i$  does not show an appreciable pattern. At strong coupling, we find two different patterns depending on  $\bar{n}$ . Figure 3(b) represents the result for a relatively low density, where  $\text{OP}_i$  oscillates in a short length (of the order of the nearest-neighbor distance) concomitantly with  $n_i$ . Figure 3(c) represents the result for a relatively high density, where  $\text{OP}_i$  oscillates in a longer length (of the order of ten sites) and shows a pattern different from that of  $n_i$  though some correlation between them is still recognizable. This result indicates a presence of another factor, in addition to  $n_i$ , determinant to the spatial structure of  $\text{OP}_i$ .

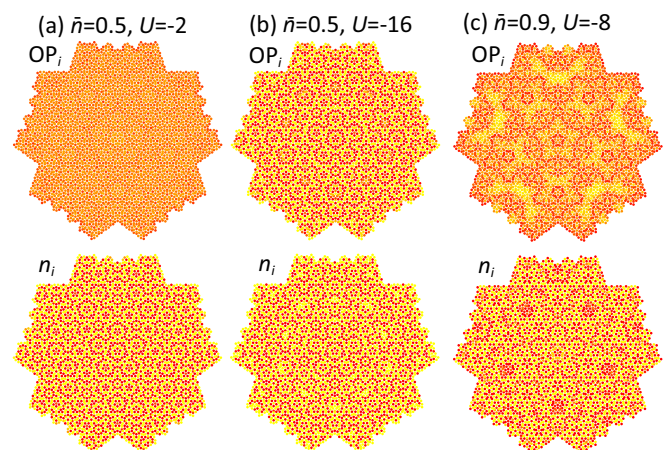


FIG. 3. Spatial patterns of  $\text{OP}_i$  and  $n_i$  at  $T = 0.01$  for three different sets of  $U$  and  $\bar{n}$ . The sites with  $Q_i > \overline{Q}$  ( $Q_i < \overline{Q}$ ) with  $Q = \text{OP}$  and  $n$  are colored by red (yellow).

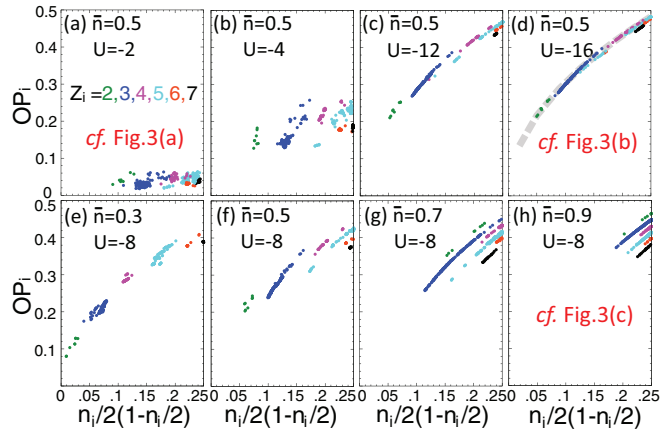


FIG. 4.  $OP_i$  plotted against  $n_i/2(1-n_i/2)$  for various sets of  $\bar{n}$  and  $U$  at  $T = 0.01$ . In order of (a)-(b)-(f)-(c)-(d),  $|U|$  increases at a fixed  $\bar{n} = 0.5$ . In order of (e)-(f)-(g)-(h),  $\bar{n}$  increases at a fixed  $U = -8$ . Thick gray dashed curve in (d) shows the result calculated for the infinite-dimensional Bethe lattice with the bandwidth  $8t$ .

This second factor is the number of bonds (the coordination number)  $Z_i$  at each site, which ranges from two to seven, depending on the local geometry of each site. To see this, in Fig. 4, we first plot  $OP_i$  against the product of the particle and hole densities  $n_i/2(1-n_i/2)$ , which is apparently related to the density of the Bogoliubov quasiparticles [51,52]; This quantity takes the maximum (0.25) for  $n_i = 1$  (half-filling) and decreases monotonously as  $n_i$  goes away from 1. We then find that the data points are well categorized by  $Z_i$  while they exhibit several different characteristics depending on  $\bar{n}$  and  $U$ .

For small  $|U|$  [Fig. 4(a)], the data points are rather scattered. However, as  $|U|$  increases in order of Figs. 4(a)-4(b)-4(f)-4(c)-4(d), all the data points merge into one curve, which increases monotonously with  $n_i/2(1-n_i/2)$ . While the extent of  $n_i/2(1-n_i/2)$  remains to be similar ( $0.05 \lesssim n_i < 0.25$ ) for all the studied values of  $U$ ,  $OP_i$  ranges considerably wider for larger  $|U|$ ;  $0.12 \lesssim OP_i \lesssim 0.26$  for  $U = -4$  and  $0.2 \lesssim OP_i \lesssim 0.5$  for  $U = -16$ .

At  $U = -16$ , each section of the curve is well grouped by  $Z_i$ : There remains a tendency that  $n_i/2(1-n_i/2)$  is larger for larger  $Z_i$ . This suggests that  $n_i$  is determined mainly by  $Z_i$  while  $OP_i$  is governed by  $n_i/2(1-n_i/2)$  (or more simply  $n_i$ ) rather than  $Z_i$  itself. This is likely because the Cooper pairs at  $U = -16$  are so strongly localized that  $Z_i$  is not directly relevant. In Fig. 4(d) we also plot the result for the infinite-dimensional Bethe lattice (with bandwidth  $8t$ ) at  $U = -16$  and  $T = 0.01$ , where the electron density is changed from 0.04 to 1.0 (gray dashed curve). Its nice agreement with the Penrose results confirms that  $OP_i$  in this region follows the behavior expected from a local physics controlled only by the electron density. Namely, provided an inhomogeneity in the electron density, the superconductivity in this region is well understood within the BEC picture.

In turn, this demonstrates that the superconductivity at smaller  $|U|$  [Figs. 4(a) and 4(b)], where the data points do not follow a simple curve, is not determined solely by the local physics and instead reflects the geometry around each site. Namely, the Cooper pairs in this region are extended

in space. Since the lack of the translational symmetry in the Penrose lattice does not allow the conventional Cooper pairing formed at the opposite Fermi momenta, this extended Cooper pairs [depicted in Fig. 3(a)] should be unconventional. We shall substantiate this point below.

By changing  $\bar{n}$  in order of Figs. 4(e)-4(f)-4(g)-4(h), we find even different characteristics in the  $OP_i$ - $n_i/2(1-n_i/2)$  plot. The structure at  $\bar{n} = 0.3$  [Fig. 4(e)] is similar to Fig. 4(d) discussed just above. Then, as  $\bar{n}$  increases with fixing  $U = -8$ , the data points overall shift to a higher value of  $n_i/2(1-n_i/2)$ , and eventually at  $\bar{n} = 0.9$ , most of the points are within  $0.2 \lesssim n_i/2(1-n_i/2) \leq 0.25$ , i.e.,  $\{n_i\}$  approaches a homogeneous distribution.

Here a caveat is needed: In general a charge order due to the attractive interaction can occur for  $\bar{n} \simeq 1$  while we have suppressed it by mixing  $g_i^0(i\omega_n)$  in Eq. (3) with the one obtained in the previous self-consistency loop. This is to focus on the inhomogeneity inherent to quasiperiodicity rather than highlighting the charge ordering which may occur particularly easily in the present bipartite lattice. In the limit of strong coupling, the present results at half-filling would be connected to the antiferromagnetic phase found in the Heisenberg model on the Penrose lattice [53–55].

In Fig. 4(h), a comparison at a fixed  $n_i$  shows that  $OP_i$  decreases with  $Z_i$ . This decrease can be explained by the curve in Fig. 2(b): The sites with large  $Z_i$  are considered to be weakly correlated compared to those with smaller  $Z_i$ , and then, according to Fig. 2(b), the former  $OP_i$  is smaller than the latter. Thus,  $OP_i$  in Fig. 4(h) is determined by  $Z_i$  rather than  $n_i$  and this is again beyond the local physics. On the other hand, the fact that for each  $Z_i$  the points follow one curve indicates the short-ranged pairs: The geometry beyond the nearest neighbors does not play a significant role (other than changing  $n_i$  slightly). This is distinct from Fig. 4(a), where a longer-range geometry beyond the nearest neighbors plays a role. We therefore conclude that the superconducting state depicted in Figs. 4(h) and 3(c) constitutes another type of unconventional superconductivity.

In order to examine the change of the spatial extent of the Cooper pairs, we calculate the off-site pair amplitude  $OP_{ij} \equiv \langle c_{i\uparrow}c_{j\downarrow} \rangle$ . Figure 5(a) plots it (after the normalization by  $\overline{OP}$ ) against the Euclidean distance  $\|\mathbf{r}_i - \mathbf{r}_j\|$  ( $\mathbf{r}_i$ : the Cartesian coordinate of site  $i$ ) for the three states in Fig. 3. For  $\bar{n} = 0.5$  and  $U = -2$  (yellow),  $OP_{ij}$  decays slowly, demonstrating that the Cooper pairs are extended in space. On the other hand, for  $\bar{n} = 0.5$  and  $U = -16$  (red) and for  $\bar{n} = 0.9$  and  $U = -8$  (blue),  $OP_{ij}$  decays much faster: The inset shows that the former decays even faster than the latter. These results support the above interpretations of the three different superconducting states.

Figures 5(b)–5(f) further clarify the nature of the Cooper pairs. Here we have defined a Fourier-transformed pair amplitude  $OP_{\mathbf{k}\mathbf{k}'} \equiv \langle c_{\mathbf{k}\uparrow}c_{\mathbf{k}'\downarrow} \rangle$ . In periodic systems,  $OP_{\mathbf{k}\mathbf{k}'}$  is finite only along the  $\mathbf{k}' = -\mathbf{k}$  line, as demonstrated in Figs. 5(b) and 5(c) for a square lattice: Figure 5(b) shows a prototype in the BCS region where  $OP_{\mathbf{k},-\mathbf{k}}$  is substantial only around the Fermi momenta, while Fig. 5(c) shows a prototype in the BEC region where  $OP_{\mathbf{k}\mathbf{k}'}$  is distributed along the  $\mathbf{k}' = -\mathbf{k}$  line.

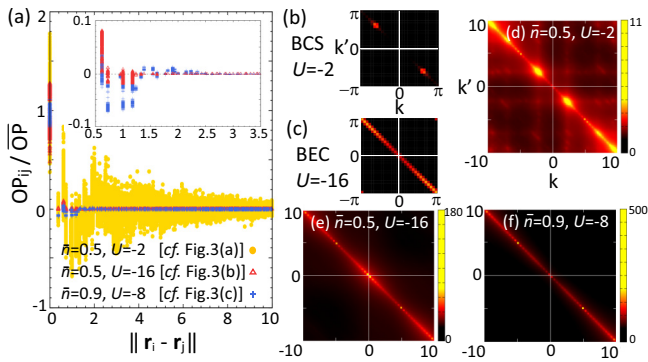


FIG. 5. (a) Off-site pair amplitude  $OP_{ij} \equiv \langle c_{i\uparrow} c_{j\downarrow} \rangle$  (normalized by  $\overline{OP}$ ) plotted against the Euclidean distance  $\|\mathbf{r}_i - \mathbf{r}_j\|$  for the three states shown in Fig. 3. Inset: Enlarged view for the short-distance part of red triangles and blue crosses. (b) and (c) Intensity map of  $|OP_{\mathbf{k}\mathbf{k}'}|$  calculated for a square lattice with the bandwidth  $8t$  at quarter filling for  $U = -2$  and  $-16$ , respectively. Just for plotting purpose, we set  $k_x = k_y = k$  and  $k'_x = k'_y = k'$ . (d)–(f) The same quantity for the three states in (a), plotted with a cutoff at  $|k|, |k'| = 10$ .

This latter BEC feature is found in Figs. 5(e) and 5(f) of Penrose, although  $OP_{\mathbf{k}\mathbf{k}'}$  is not strictly zero even for  $\mathbf{k}' \neq -\mathbf{k}$ . Meanwhile, in Fig. 5(d) several high-intensity lines are discernible besides  $\mathbf{k}' = -\mathbf{k}$ . In addition, high-intensity spots exist on the  $\mathbf{k}' = -\mathbf{k}$  line, despite that the Fermi momentum is undefined on the Penrose lattice. Because a similar structure is obtained even when we use only inner sites for the Fourier transformation, this cannot be attributed to a boundary effect. This nontrivial structure differs from a disordered BCS state, suggesting a unique pairing intrinsic to the Penrose lattice. Note that the lack of the inversion symmetry in the Penrose lattice suggests that this pairing is a mixture of spin singlet and triplet.

We summarize the results in Fig. 6. The phase diagram is calculated at  $T = 0.01$ , where only the ground state has a substantial Boltzmann weight except for  $\bar{n} \lesssim 0.3$  and/or  $|U| \lesssim 2$ . The yellow, red, and blue regions denote the superconducting states represented by Figs. 3(a), 3(b), and 3(c), respectively. In the yellow region, the Cooper pairs are spatially extended while the pairing departs from the BCS theory. The red region follows the BEC picture aside from the electron-density modulation. In the blue region, the Cooper pairs are nonlocal but short

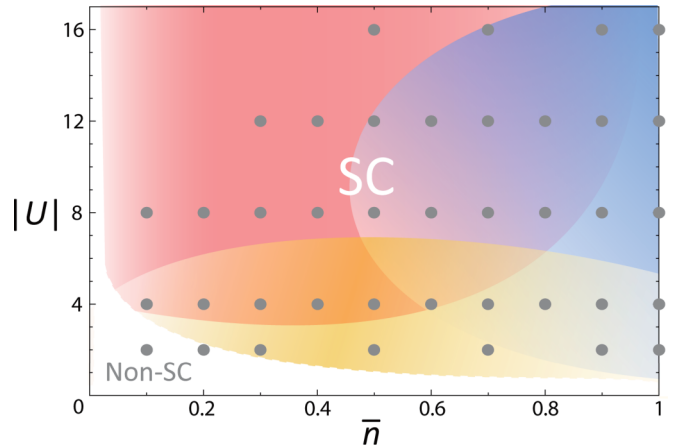


FIG. 6. Phase diagram on the  $\bar{n}$ - $U$  plane at  $T = 0.01$ . SC denotes the superconducting phase. The yellow, red, and blue regions, which are judged from the characteristics seen in the  $OP_i - n_i/2(1 - n_i/2)$  plots like Fig. 4, denote the superconducting states represented by Figs. 3(a), 3(b), and 3(c), respectively.

ranged. These three states cross over each other, as expressed by the overlaps of colors.

These results reveal that a quasiperiodic system is a fertile ground of novel superconductivity, which would become particularly fruitful when the fractal geometry interplays with the macroscopic quantum nature of superconductivity. Many issues remain open, such as a functional form of the extended non-BCS Cooper pairs, physical properties of these superconductors, and the effect of nonlocal correlations. Studies for more realistic models, with including phonons, orbital degrees of freedom, and a variation in the transfer integrals, are also an intriguing future subject.

We thank Masahito Ueda, Masatoshi Imada, and Shintaro Hoshino for stimulating discussions. S.S. is supported by JSPS KAKENHI Grants No. JP26800179 and No. JP16H06345. N.T. is supported by RIKEN Special Postdoctoral Researchers Program and by JSPS KAKENHI Grant No. JP16H07447. A.K. is supported by MEXT KAKENHI Grants No. JP25800193 and No. JP16H01066. R.A. is supported by MEXT KAKENHI Grant No. JP15H05883 and JSPS KAKENHI Grant No. JP16H06345.

[1] D. Shechtman, I. Blech, D. Gratias, and J. W. Cahn, *Phys. Rev. Lett.* **53**, 1951 (1984).  
 [2] A. P. Tsai, A. Inoue, and T. Masumoto, *Jpn. J. Appl. Phys.* **27**, L1587 (1988).  
 [3] A. P. Tsai, J. Q. Guo, E. Abe, H. Takakura, and T. J. Sato, *Nature (London)* **408**, 537 (2000).  
 [4] W. Steurer and S. Deloudi, *Acta Crystallogr. Sect. A* **64**, 1 (2008).  
 [5] M. Kohmoto and B. Sutherland, *Phys. Rev. Lett.* **56**, 2740 (1986).  
 [6] M. Arai, T. Tokihiro, T. Fujiwara, and M. Kohmoto, *Phys. Rev. B* **38**, 1621 (1988).

[7] B. Sutherland, *Phys. Rev. B* **34**, 3904 (1986).  
 [8] H. Tsunetsugu, T. Fujiwara, K. Ueda, and T. Tokihiro, *J. Phys. Soc. Jpn.* **55**, 1420 (1986).  
 [9] T. Tokihiro, T. Fujiwara, and M. Arai, *Phys. Rev. B* **38**, 5981 (1988).  
 [10] M. Kohmoto, L. P. Kadanoff, and C. Tang, *Phys. Rev. Lett.* **50**, 1870 (1983).  
 [11] S. Ostlund, R. Pandit, D. Rand, H. J. Schellnhuber, and E. D. Siggia, *Phys. Rev. Lett.* **50**, 1873 (1983).  
 [12] T. Fujiwara, *Phys. Rev. B* **40**, 942 (1989).  
 [13] H. Tsunetsugu, T. Fujiwara, K. Ueda, and T. Tokihiro, *Phys. Rev. B* **43**, 8879 (1991).

- [14] H. Tsunetsugu and K. Ueda, *Phys. Rev. B* **43**, 8892 (1991).
- [15] K. Deguchi, S. Matsukawa, N. K. Sato, T. Hattori, K. Ishida, H. Takakura, and T. Ishimasa, *Nat. Mater.* **11**, 1013 (2012).
- [16] S. Watanabe and K. Miyake, *J. Phys. Soc. Jpn.* **82**, 083704 (2013).
- [17] V. R. Shaginyan, A. Z. Msezane, K. G. Popov, G. S. Japaridze, and V. A. Khodel, *Phys. Rev. B* **87**, 245122 (2013).
- [18] E. C. Andrade, A. Jagannathan, E. Miranda, M. Vojta, and V. Dobrosavljević, *Phys. Rev. Lett.* **115**, 036403 (2015).
- [19] S. Thiem and J. T. Chalker, *Phys. Rev. B* **92**, 224409 (2015).
- [20] N. Takemori and A. Koga, *J. Phys. Soc. Jpn.* **84**, 023701 (2015).
- [21] S. Takemura, N. Takemori, and A. Koga, *Phys. Rev. B* **91**, 165114 (2015).
- [22] N. Hartman, W.-T. Chiu, and R. T. Scalettar, *Phys. Rev. B* **93**, 235143 (2016).
- [23] S. Watanabe and K. Miyake, *J. Phys. Soc. Jpn.* **85**, 063703 (2016).
- [24] J. Otsuki and H. Kusunose, *J. Phys. Soc. Jpn.* **85**, 073712 (2016).
- [25] R. Shinzaki, J. Nasu, and A. Koga, *J. Phys. Soc. Jpn.* **85**, 114706 (2016).
- [26] K. Deguchi, M. Nakayama, S. Matsukawa, K. Imura, K. Tanaka, T. Ishimasa, and N. K. Sato, *J. Phys. Soc. Jpn.* **84**, 023705 (2015).
- [27] K. M. Wong, E. Lopdrup, J. L. Wagner, Y. Shen, and S. J. Poon, *Phys. Rev. B* **35**, 2494 (1987).
- [28] J. L. Wagner, B. D. Biggs, K. M. Wong, and S. J. Poon, *Phys. Rev. B* **38**, 7436 (1988).
- [29] L. Guidoni, C. Triché, P. Verkerk, and G. Grynberg, *Phys. Rev. Lett.* **79**, 3363 (1997).
- [30] L. Guidoni, B. Dépret, A. di Stefano, and P. Verkerk, *Phys. Rev. A* **60**, R4233 (1999).
- [31] L. Sanchez-Palencia and L. Santos, *Phys. Rev. A* **72**, 053607 (2005).
- [32] F. Matsuda, M. Tezuka, and N. Kawakami, *J. Phys. Soc. Jpn.* **83**, 083707 (2014).
- [33] P. Anderson, *J. Phys. Chem. Solids* **11**, 26 (1959).
- [34] R. Penrose, *Inst. Math. Appl. Bull.* **10**, 266 (1974).
- [35] R. Micnas, J. Ranninger, and S. Robaszkiewicz, *Rev. Mod. Phys.* **62**, 113 (1990).
- [36] J. Bardeen, L. N. Cooper, and J. R. Schrieffer, *Phys. Rev.* **108**, 1175 (1957).
- [37] W. Metzner and D. Vollhardt, *Phys. Rev. Lett.* **62**, 324 (1989).
- [38] A. Georges, G. Kotliar, W. Krauth, and M. J. Rozenberg, *Rev. Mod. Phys.* **68**, 13 (1996).
- [39] M. Potthoff and W. Nolting, *Phys. Rev. B* **59**, 2549 (1999).
- [40] D. Levine and P. J. Steinhardt, *Phys. Rev. Lett.* **53**, 2477 (1984).
- [41] M. Capone, L. de' Medici, and A. Georges, *Phys. Rev. B* **76**, 245116 (2007).
- [42] A. Liebsch and H. Ishida, *J. Phys.: Condens. Matter* **24**, 053201 (2012).
- [43] S. Sakai, M. Civelli, Y. Nomura, and M. Imada, *Phys. Rev. B* **92**, 180503 (2015).
- [44] S. Sakai, M. Civelli, and M. Imada, *Phys. Rev. Lett.* **116**, 057003 (2016).
- [45] A. Garg, H. R. Krishnamurthy, and M. Randeria, *Phys. Rev. B* **72**, 024517 (2005).
- [46] A. Toschi, M. Capone, and C. Castellani, *Phys. Rev. B* **72**, 235118 (2005).
- [47] J. Bauer and A. C. Hewson, *Europhys. Lett.* **85**, 27001 (2009).
- [48] A. Koga and P. Werner, *Phys. Rev. A* **84**, 023638 (2011).
- [49] R. Peters and J. Bauer, *Phys. Rev. B* **92**, 014511 (2015).
- [50] We have confirmed the presence of the off-diagonal long-range order, by calculating the eigenvalues of the two-particle reduced density matrix.
- [51] A. Ghosal, M. Randeria, and N. Trivedi, *Phys. Rev. Lett.* **81**, 3940 (1998).
- [52] A. Ghosal, M. Randeria, and N. Trivedi, *Phys. Rev. B* **65**, 014501 (2001).
- [53] S. Wessel, A. Jagannathan, and S. Haas, *Phys. Rev. Lett.* **90**, 177205 (2003).
- [54] E. Y. Vedmedenko, U. Grimm, and R. Wiesendanger, *Phys. Rev. Lett.* **93**, 076407 (2004).
- [55] A. Jagannathan, A. Szallas, S. Wessel, and M. Duneau, *Phys. Rev. B* **75**, 212407 (2007).